

[illegible]

at the section B (the output end of the displacement amplifier), as shown in equation 1, where C_s is the coefficient stress required for the ultrasonic fatigue test, and the value can be obtained by finite element analysis. Considering the averaging output of insensitive grid to stress distribution along the specimen, even the C_s from the stress calibration is very close to that from FEA, the C_s in the FEA was used during the test.

$$\sigma_{max} = C_s A_0 \quad (S1)$$

As shown in Figure S2, based on ultrasonic axial loading fatigue, the shape and structure of the specimen are redesigned, and the connecting modules required for bending fatigue loading are added, and then a simple very-high cycle bending fatigue test system is constructed. The bending fatigue test system can convert the longitudinal vibration signal into the transverse vibration signal. Under the vibration form of cantilever bending, the maximum stress of the specimen is located at the constraint section (also the excitation section), and the constraint quality at this position will affect the initiation and propagation of bending fatigue crack. Therefore, it is necessary to consider the mode of second-order bending, and transfer the dangerous section in bending loading to the inside of the sample.

2、The strain and displacement diagrams along the A-A path.

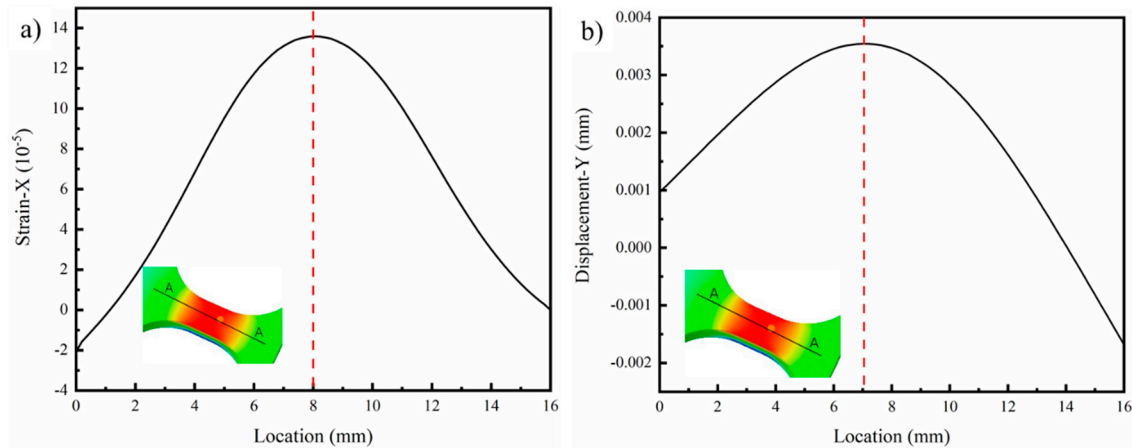


Figure S3. a) strain distribution in the gauge section under 1 μ m displacement load constraint; b) displacement distribution in the gauge section under 1 μ m displacement load constraint

3、The morphological characteristics of the fracture surface

In the region of crack initiation, crack extension in the form of short cracks depends on the

sensitivity of the microstructure [2, 3]. It is noteworthy that the length of short cracks is usually the size of one to a few grains in the rough area, while the length of microcracks is usually no more than one grain size. During the accumulation of fatigue loading, when the crack crosses the fisheye region, the crack changes from short crack extension to long crack extension [4]. To illustrate the behavior of short crack extension during crack initiation, the surface profile of the crack initiation region is obtained using laser confocal microscopy along line AB (A is the measurement position and B is the reference position) through the crack initiation region to reveal the crack driving force, as shown in Figure S4 and S5, where the red arrows represent the direction of short crack extension. The fatal short crack extension direction presents different directions relative to the fatigue loading direction, and in Figure S4, the fatal short crack is 42.5° from the loading direction. In Figure S5, the fatal short crack is at 44° with respect to the loading direction. It can be seen that the expansion direction of the short crack is close to 45° with respect to the loading direction, which means that the expansion behavior of the short crack is driven by the maximum shear stress.

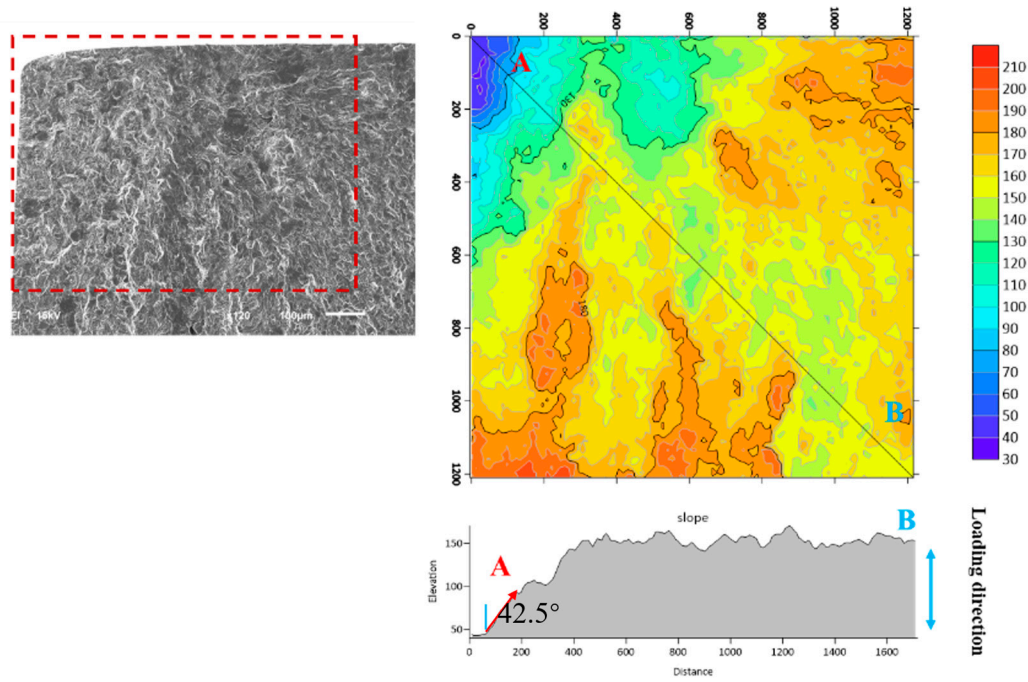


Figure S4. $\sigma_a = 390.14$ MPa and $N_f = 3.39 \times 10^5$ cycles

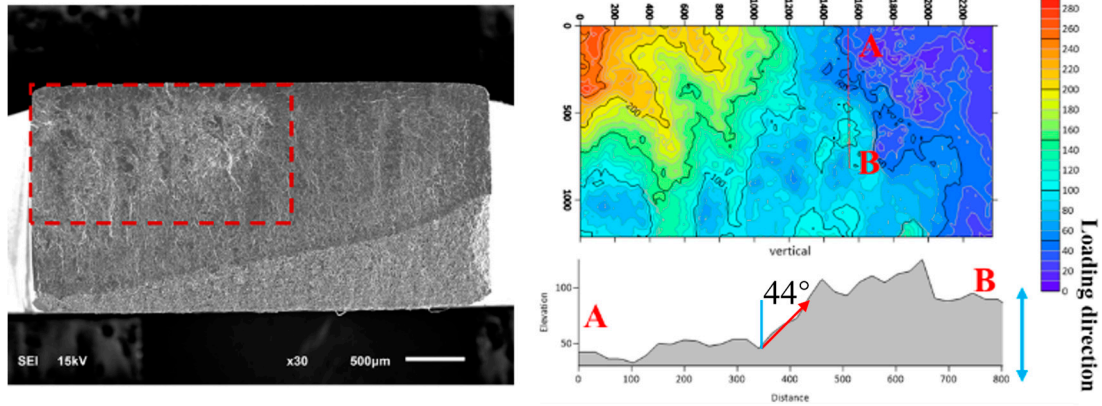


Figure S5. $\sigma_a = 246.66$ MPa and $N_f = 9.91 \times 10^7$

Reference

- [1] C. Bathias, Piezoelectric fatigue testing machines and devices, *Int J Fatigue* 28(11) (2006) 1438-1445.
- [2] F. Bridier, D.L. McDowell, P. Villechaise, J. Mendez, Crystal plasticity modeling of slip activity in Ti-6Al-4V under high cycle fatigue loading, *International Journal of Plasticity* 25(6) (2009) 1066-1082.
- [3] D.L. McDowell, F.P.E. Dunne, Microstructure-sensitive computational modeling of fatigue crack formation, *Int J Fatigue* 32(9) (2010) 1521-1542.
- [4] F. Liu, C. He, Y. Chen, H. Zhang, Q. Wang, Y. Liu, Effects of defects on tensile and fatigue behaviors of selective laser melted titanium alloy in very high cycle regime, *Int J Fatigue* 140 (2020).